RSC Advances

PAPER

View Article Online
View Journal | View Issue

Cite this: *RSC Adv.*, 2015, **5**, 82605

Large strain response and fatigue-resistant behavior in lead-free $Bi_{0.5}(Na_{0.80}K_{0.20})_{0.5}TiO_3$–$(K_{0.5}Na_{0.5})MO_3$ (M = Sb, Ta) ceramics

Jigong Hao, Zhijun Xu,* Ruiqing Chu, Wei Li, Juan Du and Peng Fu

Received 6th July 2015
Accepted 22nd September 2015

DOI: 10.1039/c5ra13126j

www.rsc.org/advances

$(1 - x)Bi_{0.5}(Na_{0.80}K_{0.20})_{0.5}TiO_3$–$x(K_{0.5}Na_{0.5})MO_3$ (M = Sb, Ta) (BNKT20–KNM100x) lead-free piezoelectric ceramics were designed and fabricated using a conventional fabrication process to achieve large strain response in BKNT20-based ceramics. The KNM substitution was found to induce a transition from ferroelectric to relaxor pseudocubic phase, and such transition is accompanied with the significant disruption of ferroelectric order and the shift of the ferroelectric–relaxor transition temperature T_{F-R} down to room temperature. Accordingly, large electric-field-induced strains of 0.39–0.41% (at 80 kV cm^{-1}, equivalently 488–513 pm^{-1} V), which are derived from a reversible field-induced ergodic relaxor to ferroelectric phase transformation, were obtained in 1.25 mol% KNM-modified compositions near the phase boundary. Moreover, an attractive property for application as actuators was obtained in the present system, compositions near the phase boundary with an ergodic relaxor state exhibited fatigue-free behavior after 10^6 cycles. Furthermore, unexpected almost fatigue-free behavior was also observed in 0.5 mol% KNM-modified samples with a typical ferroelectric long-range order. Results of the enhanced activation energy (E_a) for electrical conduction suggest the well-observed fatigue-resistant behavior in the present system should be mainly attributed to the lower defect density. These findings give the current material great opportunity for actuator applications demanding improved cycling reliabilities.

1. Introduction

Recently, increasing demand for environmentally friendly materials in electronic industry promotes a wide range of studies on lead-free piezoelectric ceramics to replace lead zirconate titanate (PZT)-based ceramics. Great attention has been paid to $(Bi_{0.5}Na_{0.5})TiO_3$ (BNT)-based perovskite ceramics in expectation of large-stroke actuator applications such as fuel injectors and vacuum circuit breakers[1] since a large electromechanical strain response comparable with some PZT-based antiferroelectric ceramics has been found in BNT-based lead-free piezoceramics[2–22] with the observation of a composition-induced ferroelectric–ergodic relaxor phase transition. Interestingly, the emergence of this large strain is at the expense of poling-induced piezoelectricity. Jo *et al.*[3] proposed that the origin of the large strain observed in the BNT-based systems can be attributed to a reversible ergodic relaxor to ferroelectric phase transformation under electric fields due to their comparable free energies.

Generally, to achieve optimized strain properties in BNT-based system, a proper choice of base composition and effective chemical modifier is very important.[4] The base BNT-based composition should have inherently large poling strain, and the long-range ferroelectric order can be disrupted with chemical modifications in a way that its reestablishment is achievable by the application of electric field.[3] A common strategy so far was to incorporate a small amount of additional chemical entities such as single isovalent dopants[5,6] donors[7–9] or ABO_3-type compounds[2–4,10–20] into BNT–$BaTiO_3$ (BT) or BNT–$(Bi_{0.5}K_{0.5})TiO_3$ (BKT) solid solution systems at the morphotropic phase boundary (MPB). In addition, creation of moderate A-site vacancies in the MPB compositions (BNT–BT or BNT–BKT) can also be helpful for achieving large strain response.[21,22] Compared with BNT–BT, BNT–BKT seems more attractive as a base composition for achieving giant strain response since it is known that this system has good piezoelectric performance with large poling strain at its MPB at approximately 20 mol% BKT.[4,12]

Furthermore, it is disclosed that an enhancement of the strain in BNT-based materials is accompanied by the disruption of ferroelectric order and the formation of ferroelectric–ergodic relaxor phase boundary. Our recent studies[14,20] provided a guideline for the detection of ferroelectric–ergodic relaxor (F–R) phase boundary in (BNT–BKT)-based systems: the position of F–R phase boundary in (BNT–BKT)-based system was related to the tolerance factor t of the adding ABO_3 member [t is a concept

College of Materials Science and Engineering, Liaocheng University, Liaocheng 252059, People's Republic of China. E-mail: zhjxu@lcu.edu.cn; Fax: +86-635-8230923; Tel: +86-635-8230923

for the arrangement of interpenetrating dodecahedra and octahedra in a ABO_3 perovskite structure, as given by, $t = (R_A + R_O)/\sqrt{2}(R_B + R_O)$, where R_A, R_B, and R_O are the ionic radii of cation A, B and oxygen, respectively[23]], and the phase boundary shifts to a (BNT–BKT)-rich part as t of ABO_3 increases, which is quite consistent with that of BNT-based binary systems.[24] In addition, we found the end ABO_3 member having a high tolerance factor >1.0 is much easier to induce the formation of the F–R phase boundary and produce a higher strain in (BNT–BKT)-based system. In this regards, $(K_{0.5}Na_{0.5})NbO_3$ (KNN) (t = 1.011) is an effective end member to BNT–BKT, which can produced a giant strain response of 0.46% at 80 kV cm^{-1} driving field, equivalently 575 pm^{-1} V.[12]

$(K_{0.5}Na_{0.5})TaO_3$ (KNT) is perovskite type material with room temperature paraelectric cubic crystal structure,[25] and $(K_{0.5}Na_{0.5})SbO_3$ (KNS) is pseudoilmenite structure.[26] both them have nearly equal tolerance factor t to that of KNN. Therefore, it is expected that the addition $(K_{0.5}Na_{0.5})MO_3$ [KNM, (M = Sb, Ta)] will distort the local structure of BNT–BKT and result in enhancement of the electric-field strain. In the present study, we selected 0.8BNT–0.2BKT (BNKT20) as a base material with small amounts of KNM being introduced as doping species. Through the addition of a proper amount of KNM, large strains of 0.39–0.41% with fatigue-resistant behavior are obtained at 80 kV cm^{-1} with a KNM content of 1.25 mol%. The temperature stability and fatigue behavior of this large strain are additionally investigated.

2. Experimental

The produced materials $(1 - x)Bi_{0.5}(Na_{0.80}K_{0.20})_{0.5}TiO_3$–$x(K_{0.5}Na_{0.5})MO_3$ (M = Sb, Ta) (abbreviated as KNM100x, M = Sb, Ta) were prepared by the conventional ceramic fabrication technique using reagent-grade metal oxides or carbonate carbonate powders of Bi_2O_3 (99.975%), TiO_2 (99.6%), Ta_2O_5 (99.99%), Sb_2O_5 (99.98%), Na_2CO_3 (99.995%) and K_2CO_3 (99.0%) as raw materials. For each composition, the starting materials were weighed according to the stoichiometric formula and ball milled for 24 h in ethanol. The dried slurries were calcined at 850 °C for 4 h and then ball milled again for 24 h. The resulting powders were then mixed with 10% polyvinyl alcohol (PVA), and pressed into pellets of 10 mm diameter and 0.8–1.0 mm thickness. After burning off the PVA, the disk samples were sintered at 1140–1160 °C in covered alumina crucibles for 2 h. To minimize the evaporation of Na, K, and Bi elements, the samples were embedded in atmospheric powder of the same composition.

Phase structure of the ceramics was identified by using X-ray diffraction (XRD, Bruker D8 Advance, Karlsruhe, Germany) with Cu K_a radiation. The microstructure of the ceramics was observed by scanning electron microscopy (SEM) (JSM-6380, Japan) on polished and thermally etched surfaces. For the electric measurements, silver paste was coated on both sides of the sintered samples and fired at 650 °C for 10 min to form electrodes. The temperature dependences of the dielectric properties were measured using an Agilent 4294A precision impedance analyzer (Agilent Inc., USA). Thermally stimulated depolarization currents (TSDC) were measured on poled samples using aix-ACCTTF2000FE-HV ferroelectric test unit (aix-ACCT Inc., Germany) at the same heating rate of 5 °C min^{-1} to determine the depolarization temperature (T_d). Impedance spectroscopy of the samples was performed using a broad frequency dielectric spectrometer (Concept80, Novocontrol Inc., Germany) in the 0.01 Hz to 20 MHz frequency range at various temperatures. The electric-field-induced polarization (P–E) and strain (S–E) measurements were carried out using an aix-ACCTTF2000FE-HV ferroelectric test unit (aix-ACCT Inc., Germany) connected with an accessory laser interferometer vibrometer (SP-S 120/500; SIOS Mebtechnik GmbH, Ilmenau, Germany). To study the fatigue behavior of the ceramics, the samples were fatigued with a positive unipolar/bipolar sine electric signal with the amplitude of 80 kV cm^{-1} at 10 Hz up to 10^6 cycles. For the measurement of piezoelectric properties, samples were poled in silicone oil at RT under a dc electric field from 50 to 60 kV cm^{-1} for about 20 min. The piezoelectric constant d_{33} was measured using a quasi-static d_{33} meter (YE2730 SINOCERA, China).

3. Results and discussion

Fig. 1 shows the XRD patterns of the KNM100x (M = Sb, Ta) ceramics. In agreement with the previous study,[25] KNM0

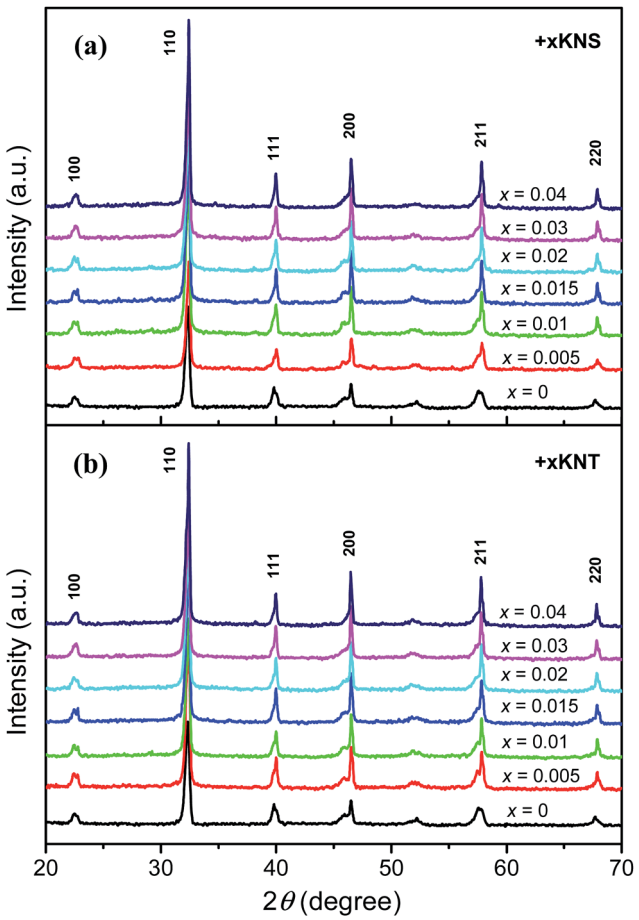

Fig. 1 XRD patterns of the KNM100x [(a) M = Sb, (b) M = Ta] ceramics.

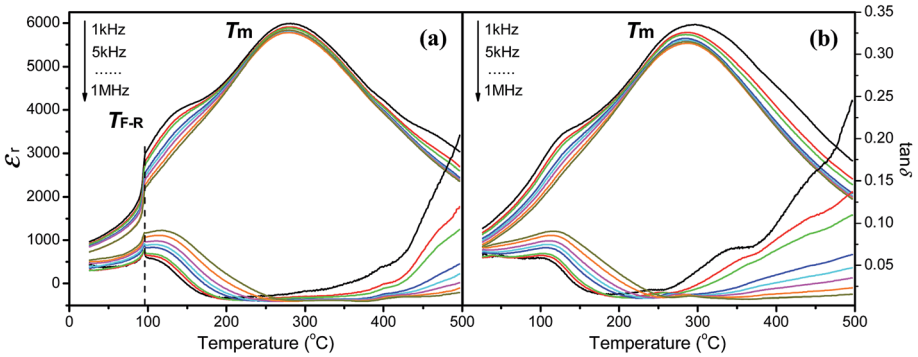

Fig. 2 Temperature dependence of dielectric constant and loss tangent for both (a) poled and (b) unpoled BNKT20 samples.

ceramic reveals peak splittings at around 46° of (002)/(200) reflections, which indicates the coexistence of rhombohedral and tetragonal phases. As KNM increases, the rhombohedral and tetragonal distortion gradually diminishes, as the split (002)/(200) peaks of the coexisted phases finally merge into a single (200) peak at higher KNS or KNT content. The result suggests that the crystal structure of the KNM100*x* evolves from the rhombohedral–tetragonal coexisted phases to a pseudo-cubic symmetry as the content of KNM increases.[14]

Fig. 2 provides temperature dependence of dielectric constant and loss tangent for both (a) poled and (b) unpoled KNM0 samples, respectively, which are representative for all ferroelectric compositions. Two dielectric anomalies are observed for both poled and unpoled samples. Meanwhile, they are also reflected in the corresponding loss tangent curves. These broad and frequency dependent peaks in dielectric constant and loss tangent indicate that KNM0 samples exhibit relaxor characteristics.[26] The dielectric maximum around 300 °C (T_m), provides a tetragonal to a cubic phase transition, and the other dielectric anomaly at lower temperatures T_{r-t}, denotes the rhombohedral–tetragonal phase transition.[24,27] While recently, it has been proposed that T_m is related to a relaxation of tetragonal polar nanoregions (PNRs) emerged from rhombohedral PNRs, which has nothing to do with measurable structural transition.[28] For poled specimens, the dielectric anomaly at lower temperatures is due to thermal evolutions of discrete PNRs, and it denotes the transition from ferroelectric-to-relaxor state,[29] where the ferroelectric-to-relaxor transition point, T_{F-R} can be determined by the frequency independent peak in the dissipation factor.[28] Generally, T_{F-R} obtained from

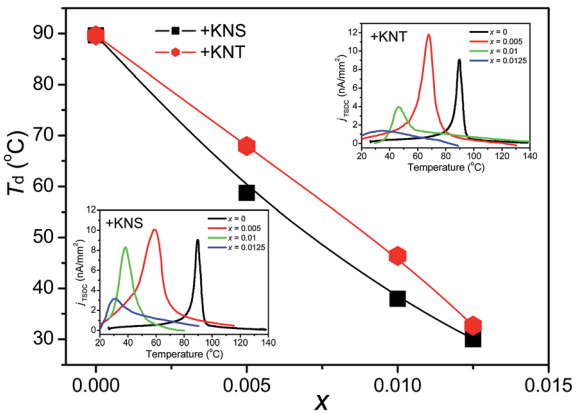

Fig. 4 Compositional dependence of T_d as a function of x for KNM100x ceramics (inset is temperature dependence of depolarization current j_{TSDC} for poled BNKT20–xKNM samples).

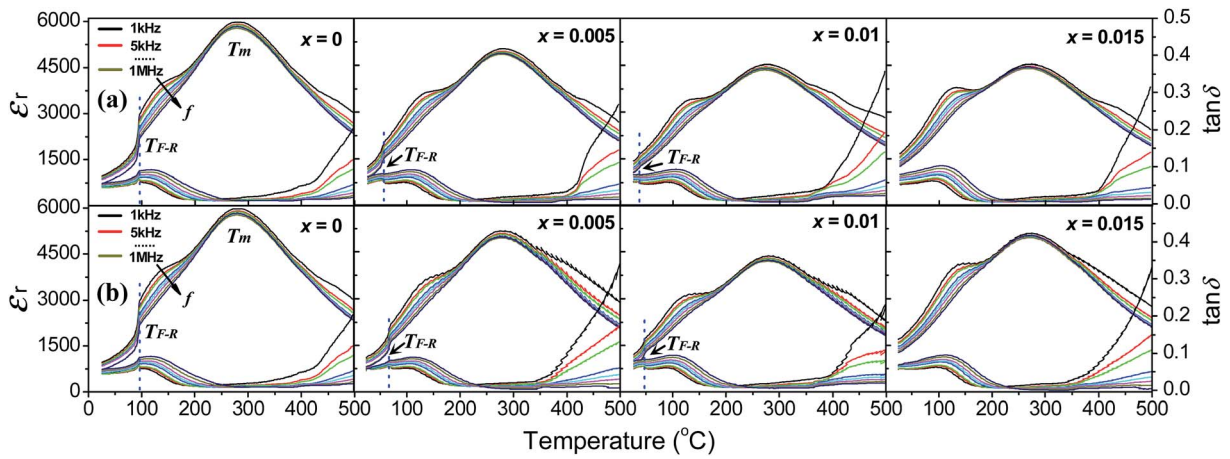

Fig. 3 Temperature dependence of dielectric constant and loss tangent for poled KNM100x [(a) M = Sb, (b) M = Ta] samples.

dielectric measurement had also been referred to as depolarization temperature T_d,[21,27] however, recent study[26] demonstrated that the difference between T_{F-R} and T_d, where T_d is measured by thermally stimulated depolarization currents (TSDC) and is a little bit lower than the previously determined T_{F-R} value.

Fig. 3 shows the temperature dependence of dielectric constant and loss tangent for poled KNM100x (M = Sb, Ta) samples. The measurement frequency ranges from 1 kHz to 1 MHz, and the dash line indicate the determined T_{F-R}. It can be seen clearly that T_{F-R} shifts gradually down to RT with the increase of KNM content. Fig. 4 gives the variation of T_d with KNM content, and insets show the temperature dependence of depolarization current (j_{TSDC}) for poled KNM100x (M = Sb, Ta) samples. Similar to the variation of T_{F-R} with KNM content, it is noted that the T_d determined from the peak in j_{TSDC} is also shifted down to RT by increasing the KNM content. In the present work, the downward shift of T_{F-R} and T_d with increasing KNM content indicates a compositionally induced ferroelectric-to-relaxor phase transition. Due to the formation of ferroelectric–ergodic relaxor phase boundary, optimized strain response can be expected in a critical composition.

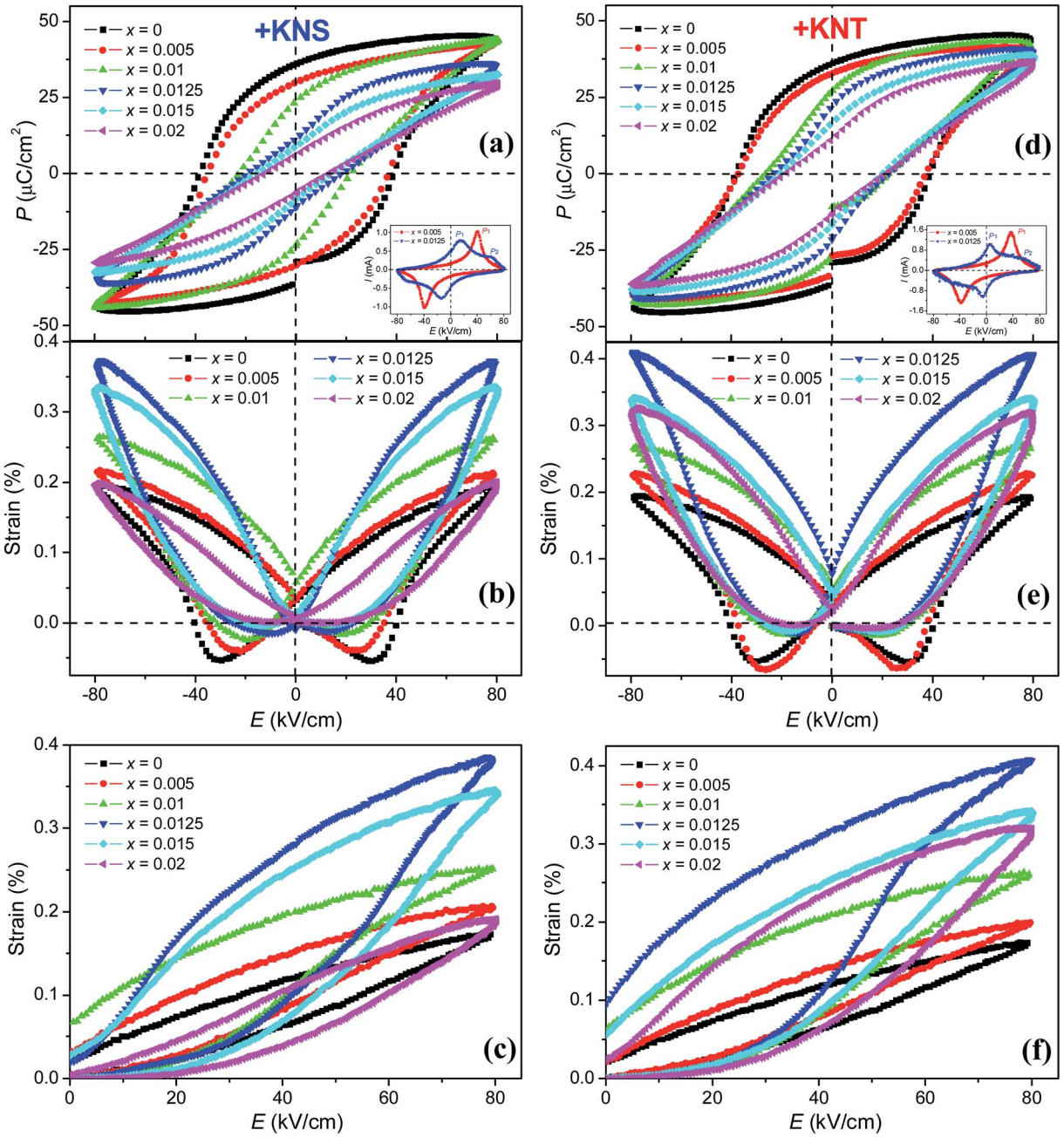

Fig. 5 Changes in the polarization hysteresis loops and bipolar/unipolar strain hysteresis loops of KNM100x (M = Sb, Ta) system measured at RT and 10 Hz.

Fig. 5 shows the changes in the polarization hysteresis loops and bipolar/unipolar strain hysteresis loops of KNM100x (M = Sb, Ta) system measured at RT and 10 Hz. It is evident that KNM0 sample exhibits a typical ferroelectric behavior with butterfly shaped strain hysteresis loop and visible negative strain S_{neg} (the definition for S_{neg} can be found in ref. 16 and [30]). A sharp polarization current peak (denoted as P_1) ascribed to the domain switching could be observed at the coercive field E_c, as shown in the inset of Fig. 5(a) and (d). In contrast, a significant reduction in the coercive field E_c is denoted in samples with a small amount of KNM addition ($x = 0.01$) with a slight trace of constriction, whereas the maximum polarization P_{max} is essentially unchanged. It indicates that the ferroelectric activity is softened with a small amount of KNM addition. Besides, a trace of pinching an also be observed for samples with 0.01KNM addition. An additional increment of KNM content to 1.25 mol% significantly disrupted the long-range ferroelectric order with an appearance of the pinched P–E loops along with an additional current peak P_2, and the constricted feature indicates the development of ergodic relaxor phase at zero field.[3]

The compositionally induced ferroelectric to ergodic relaxor phase transformation with the addition of KNM is also verified by bipolar strain measurements, as shown in Fig. 5(b) and (e). With the increasing KNM content, S_{neg} disappears where the pinching takes place in the polarization hysteresis, together with a concurrent increase in the total bipolar strain level (S_{bi}). These changes also indicate a pronounced increase in the strain that is expected to contribute to the unipolar strain (S_{uni}). In fact, a drastic increase in the S_{uni} up to 0.39% (KNS1.25) and 0.41% (KNT1.25) is observed in these compositions, as shown in Fig. 5(c) and (f). The shape of the unipolar strain curves clearly visualizes the underlying mechanism for the enhanced strain value, which is in good conformity with the previous observation made on the BNT-based ceramics.[2–6,8–15] For samples with $x \leq 0.01$, the unipolar strain curve shows an almost linear increase with electric field, which is usual in normal ferroelectric materials such as PZT. The smaller hysteresis with a linear strain response in these samples shows a large amount of intrinsic contributions to the strain response. However, as the KNM content increases up to 0.0125, large variation takes place in the strain, which increases quadratically from 0 until it culminates at around 40 kV cm^{-1} and again decreases quadratically with decreasing electric field. The large degree of piezoelectric hysteresis in samples with KNM1.25 shows that the high strain level in the present work is aligned with an effective piezoelectric response, which mainly derived from extrinsic effects while less from intrinsic contribution.[13]

Fig. 6(a) gives the composition dependence of negative strain S_{neg} and unipolar strain S_{uni} strain value, showing an apparent correlation between the negative strain S_{neg} and unipolar strain S_{uni}: a large negative strain S_{neg} reduces the potential for a material to display large strains upon unipolar electric loading.[31] Fig. 6(b) shows the composition dependence of the quasi-static d_{33} and normalized strain d^*_{33} (S_{max}/E_{max}). It is interesting that an abrupt drop in d_{33} is simultaneously observed at 0.0125KNM, where the largest d^*_{33} of 488 pm^{-1} V (KNS1.25) and 513 pm^{-1} V (KNT1.25) are obtained. At this point, specimens show little piezoelectric responses, confirming an ergodic relaxor phase states in this material.

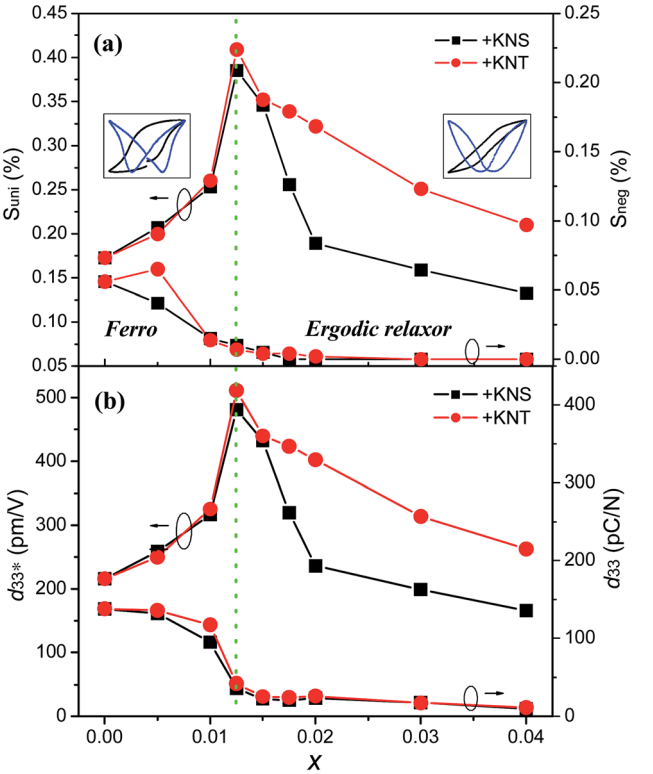

Fig. 6 (a) Composition dependence of negative strain S_{neg} and unipolar strain S_{uni}. (b) Composition dependence of the quasi-static d_{33} and normalized strain d^*_{33} (S_{max}/E_{max}) of KNM100x ceramics.

To further analyze the phase transition behavior in the KNM100x (M = Sb, Ta) system, the small-signal parameters ε_{33} and d^*_{33} of the samples were measured, as presented in Fig. 7. Ferroelectric compositions KNM100x ($x \leq 0.01$) exhibit notable hysteretic behavior in ε_{33}–E curves, which is closely connected to switching of ferroelectric domains.[18] Furthermore, the d^*_{33}–E curves of the two samples resembles their P–E loops. It is also noted that no prominent peak of d^*_{33} is observed near the E_c for the KNM100x ($x \leq 0.01$) samples, which is indifferent from the soft PZT, where a sharp maximum in ε_{33} near the E_c results in a maximum in d^*_{33}. By contrast, ergodic relaxor KNM100x ($x \geq 0.015$) samples display indiscernible hysteretic behavior with slim ε_{33}–E and d^*_{33}–E, indicating little domain switching.[18]

Suitable materials for piezoelectric applications not only show excellent properties but also have to be reliable under long-term electric cycling.[32,33] Recently, large strain response was reported in many BNT-based systems.[2–22] Nevertheless, electrical fatigue on BNT-based lead-free piezoelectric systems receives quite little attention and only few studies have been published.[34–38] PZT is known to exhibit poor piezoelectric fatigue properties with relatively severe degradation in strain behavior after only a few millions of cycles of applied field, while the completely electrostrictive rhombohedral phases of La-doped PZT behavior were shown to be fatigue free up to 10^6 cycles.[39] More recently, MPB compositions of 0.94BNT–0.06BT

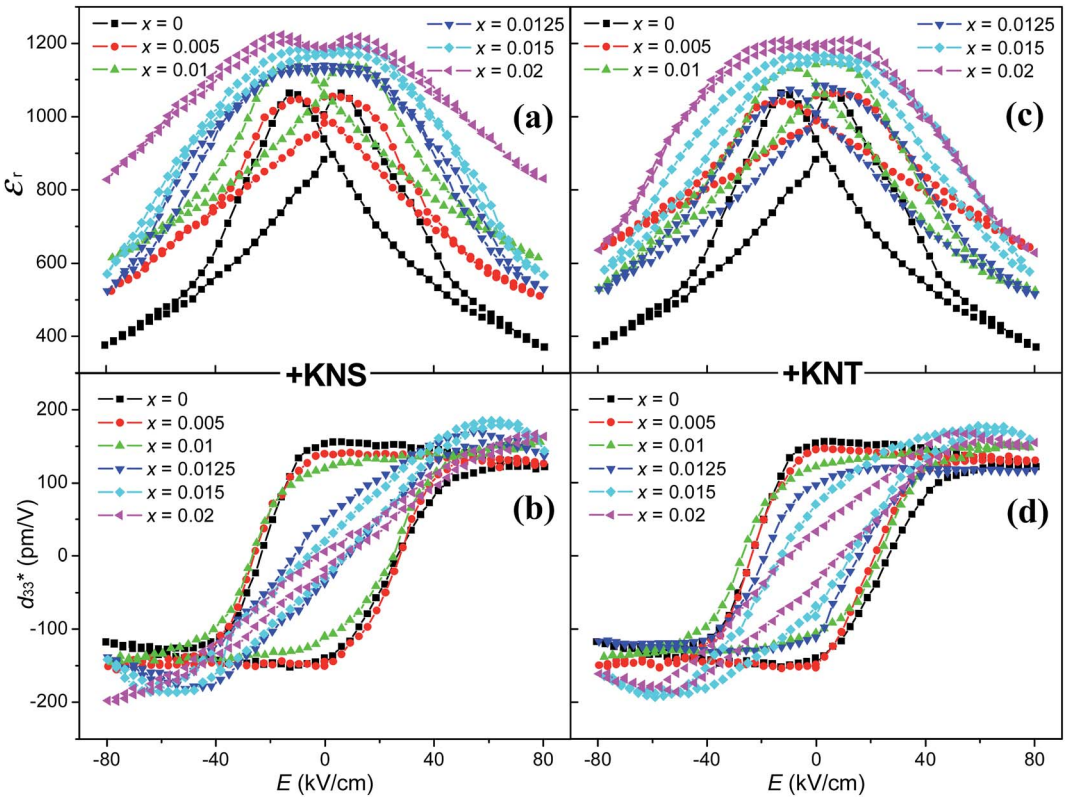

Fig. 7 The small-signal parameters (a), (c) ε_{33} and (b), (d) d_{33}^* of KNM100x (M = Sb, Ta) samples under high bias fields up to 80 kV cm^{-1}.

have been investigated for piezoelectric fatigue. Results showed the polarization dropped by 47.4% of the initial value after 1000 cycles. Proper amount of CuO acted to stabilize the rhombohedral phase into a tetragonal phase and improved the fatigue characteristics without negatively impacting the piezoelectric response.[34] These findings suggested that the fatigue property of the sample was related to its phase structure. In the present work, we selected two kinds of samples with different phase structures (ferroelectric and ergodic relaxor) to study the relation of fatigue characteristics and phase structure. The results are presented in Fig. 8 and 9.

Fig. 8 shows the unipolar fatigue behavior of ferroelectric (a) KNM0, (b) KNT0.5 and ergodic relaxor (c) KNT1.25, (d) KNS1.25 ceramics measured at a frequency of 10 Hz for 10^6 cycles. The unipolar strain levels at different unipolar fatigue cycles for the above samples are summarized in Fig. 8(e). For the ferroelectric KNM0, the electromechanical strain value shows relatively small, but consistent decreases of approximately 11.5% in the unipolar strain S_{uni}, from 0.180% to 0.153%, after 10^6 cycles. This decrease, however, is quite minimal when compared to the reduced strain and significant hysteresis asymmetry seen in previously published work on PZT.[39,40] While for ferroelectric KNT0.5, it shows an enhanced fatigue behavior with only a 6.0% decrease of S_{uni}. By contrast, ergodic relaxor KNT1.25 and KNS1.25 materials exhibit large strains double of that of the ferroelectric KNM0 and KNT0.5 samples, together with fatigue-free behavior up to 10^6 switching cycles: the general variation of the S_{uni} up to 10^6 cycles is within ~2.3% of original value. That is to say the ergodic relaxor phase stabilizes the unipolar fatigue behavior.

To understand the behavior of the unipolar strain during electrical cycling more in detail, bipolar hysteresis loops of polarization P and strain S were recorded in the unfatigued state and after distinct cycling steps. The evolution of polarization P–E and bipolar strain S–E hysteresis loops of ferroelectric (a and b) KNM0, (c and d) KNT0.5 and ergodic relaxor (e and f) KNT1.25, (g and h) KNS1.25 ceramics are displayed in Fig. 9. Following the completion of one million cycles of fatigue at 80 kV cm^{-1}, clear trends can be observed in the polarization and strain hysteresis data, for ferroelectric KNM0 ceramics. Although the symmetry of the strain hysteresis is maintained upon completion of the fatigue cycling, the electromechanical strain is seen to decrease from approximately 0.182% to 0.149%, a decrease of approximately 18.1%. In the case of remanent polarization (P_r), the similar effect is observed with a slightly larger decrease of 19.8% in this sample. For ferroelectric KNT0.5, it is noted that this material is less sensitive to bipolar fatigue loading: there is a small variation in the remnant polarization P_r (3.0%) and electromechanical strain S (the average value is 4.5%). In contrast, ergodic relaxor KNT1.25 and KNS1.25 samples render fatigue process stable and nearly no fatigue degradation is noted: the materials with giant strain finally exhibit almost no quantifiable degradation even with fatigue loading at 80 kV mm^{-1} for 10^6 cycles.

When compared to traditional PZT,[42,43] a significant improvement on the fatigue response was obtained in present

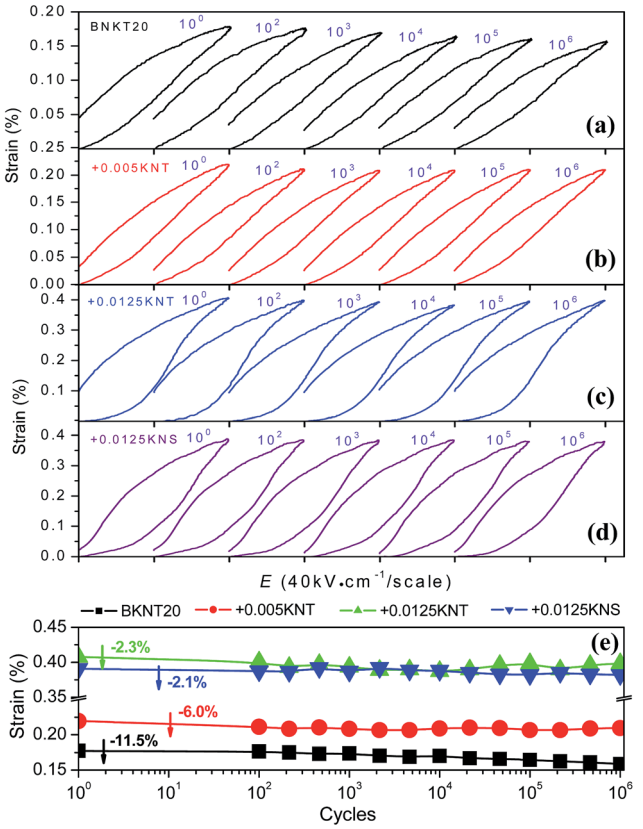

Fig. 8 Unipolar fatigue behavior of ferroelectric (a) BNKT20, (b) KNT0.5 and ergodic relaxor (c) KNT1.25, (d) KNS1.25 ceramics measured at a frequency of 10 Hz for 10^6 cycles. (e) The unipolar strain levels at different unipolar fatigue cycles for the above samples.

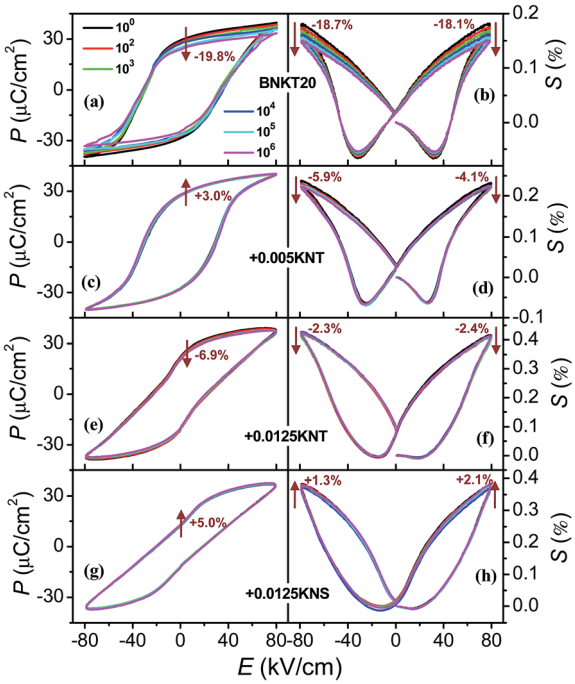

Fig. 9 The evolution of polarization P–E and bipolar strain S–E hysteresis loops of ferroelectric (a and b) BNKT20, (c and d) KNT0.5 and ergodic relaxor (e and f) KNT1.25, (g and h) KNS1.25 ceramics.

KNM100x system. Fig. 10 depicts the fatigue behavior of KNT1.25 in relation to the degradation characteristics of a commercial soft PZT with the composition $Pb_{0.99}[Zr_{0.45}Ti_{0.47}(Ni_{0.33}Sb_{0.67})_{0.08}]O_3$ (PIC151 from PI Ceramics, Lederhose, Germany)[42] under 10^7 cycling conditions. Inset shows the unipolar strain curves of KNT1.25 ceramics under different unipolar fatigue cycles. The general variation of the strain for KNT1.25 up to 10^7 cycles is within 3% of original value. In contrast to that, PIC151 experiences approximately 15% reduction in strain behavior after 10^7 electric cycles. In traditional lead-based system, the pinning of domain walls by stress, point defect, space charge field, microcracks or macrocracks, and field screening due to damaged material accumulated around the electrode region played an important role in the fatigue behavior.[40–43] However, the fatigue models for the traditional PZT ceramics appeared to be quite weak for the present KNM100x system. Regarding to the intrinsic mechanism responsible for the observed fatigue-free behavior, several mechanisms such as the combined effects of the symmetry variation and decrease in the local charges, and a reversible field-induced phase transition have been proposed.[34,36,44–46] These explanations could indeed account to some extent for the ferroelectric fatigue-free behavior of lead-free solid solutions with a specific order state. For the BNT-based ceramics with ergodic relaxor phase, *e.g.* BNT–BT–$SrTiO_3$,[37] BNT–BT–$Bi(Zn_{0.5}Ti_{0.5})O_3$,[38] BNT–BT–KNN,[47] the improved fatigue property can be attributed to the reversible field-induced phase transition between the ergodic relaxor pseudocubic and ferroelectric phase along with the low concentration of defects.[37,38,48] These explanations could be able to explain the ferroelectric fatigue-free behavior of the studied KNT1.25 and KNS1.25 samples with ergodic relaxor state. Nevertheless, for the present ferroelectric KNM0 and KNT0.5, they exhibited much different fatigue characteristic, although both them exhibit typical

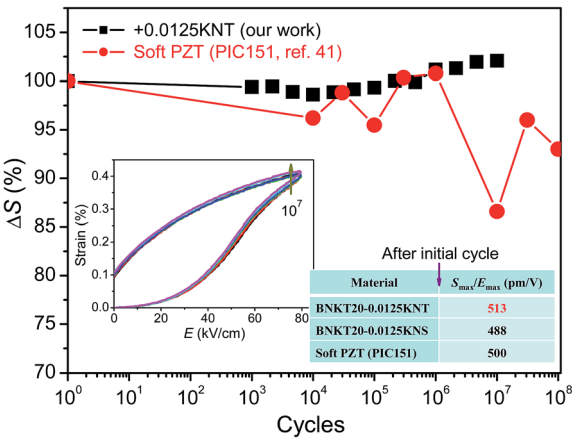

Fig. 10 Unipolar strain deviations ΔS of KNT1.25 ceramics as a function of cycles with the data of a soft commercial PZT (PIC151) provided for comparison.[41] Inset shows the unipolar strain curves of KNT1.25 ceramics under different unipolar fatigue cycles.

ferroelectric behavior. It is therefore quite necessary to clarify the intrinsic reason.

It is well known that intrinsic defects play an important role in the fatigue behavior of the perovskite ferroelectric materials. In the present work, complex impedance spectra were characterized to give an insight into the defect type and electrical conductivity. Fig. 11(a) shows the complex impedance spectra of the KNM100x (M = Sb, Ta) ceramics with $x = 0.005$, 0.0125, 0.02 and 0.04 in the frequency range of 0.01 Hz to 20 MHz over 500–650 °C. The results of pure KNM0 sample can be can be referenced in our recent work.[48] Commonly, electrode, grain boundary and grain components contribute to the conductivities of the polycrystalline materials and their effects on conduction can be segregated into three parallel RC elements connected in series in an equivalent circuit, from low frequency to high frequency.[49] For the studied samples, there is only a single, substantially undistorted Debye-like semicircle observed, indicating that all the sample contains essentially one electrical component associated with the grain effect in the measured temperature range. Upon heating, the semicircles gradually shift to the real axis (Z'). This behavior can be assigned to the activation of the weakly trapped charge carriers, which results in the increase in conductivity (σ).

Fig. 11(b) shows the logarithms of conductivities (σ) *vs.* 1000/T of the KNM100x (M = Sb, Ta) ceramics. From which, the activation energy (E_a) for electrical conduction can be detected by using the Arrhenius equation:

$$\sigma = \sigma_0 \exp(-E_a/kT) \quad (1)$$

where σ and σ_0 are the dc conductivity and the pre-exponent constant, respectively, E_a is the activation energy, k is Boltzmann's constant, and T is absolute temperature. The solid lines are the best least-squares fitting of eqn (1). In ABO_3 perovskite materials, the values of E_a for A- and B-site cations are around 4 and 12 eV, respectively.[50] For oxygen vacancies, it varies from 0.5 to 2 eV, depending on their concentration.[51] In the present work, the achieved E_a of KNM100x are in the range of 1.68–1.79 eV, which are closely related to the oxygen ion/vacancy migration. Therefore, it is reasonable to suggest that oxygen vacancies dominate the conductivity in this temperature range from 550 to 650 °C. Compared with the E_a of PZT ceramics ($E_a = 1$ eV),[52] all the samples exhibited a much higher E_a, indicating the decreased oxygen vacancies compared to the PZT ceramics. The lower oxygen concentration may be attributed to the lower sintering temperature of the present KNM100x solid solution which would lead to a lower defect density compared to the PZT system. Therefore, the greatly enhanced fatigue properties in the present KNM100x system should be attributed to the lower defect density.[36–38] Furthermore, for the present ferroelectric KNM0 and KNT0.5, the E_a was determined to be 1.55eV (ref. 48)

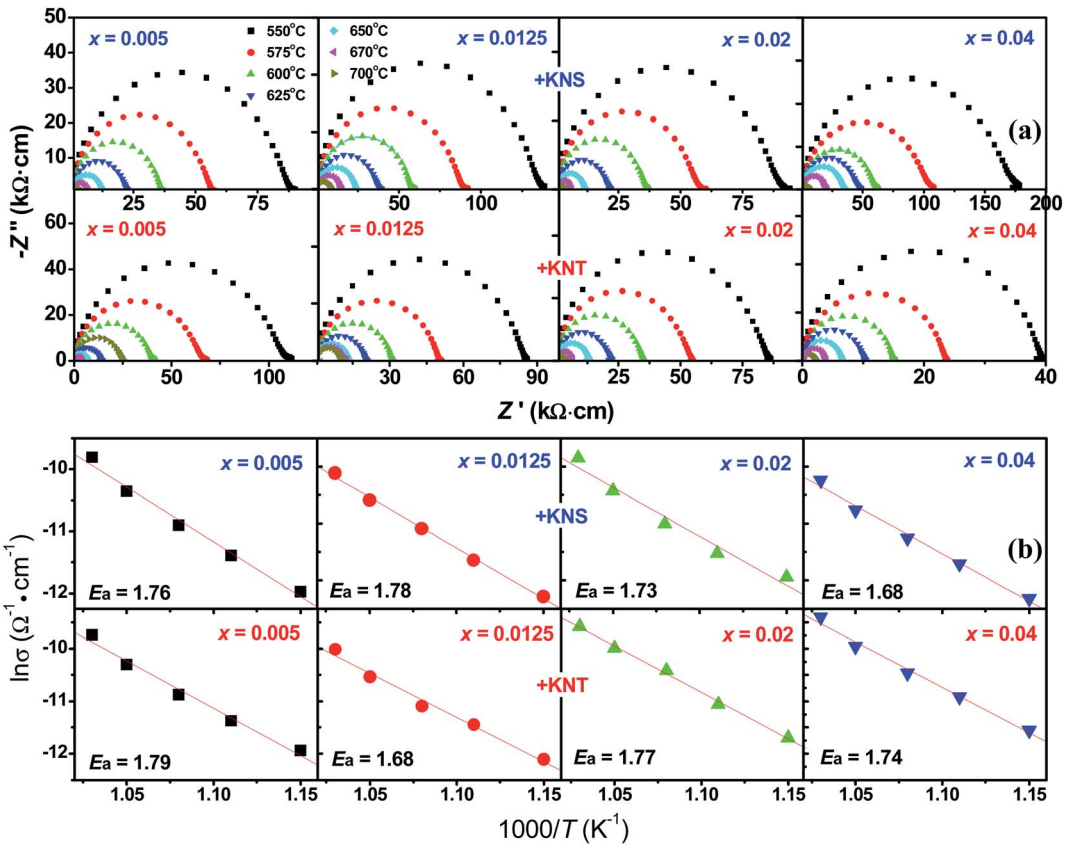

Fig. 11 (a) Complex impedance spectra of the KNM100x (M = Sb, Ta) ceramics with $x = 0.005$, 0.0125, 0.02 and 0.04 in the frequency range of 0.01 Hz to 20 MHz over 500–650 °C. (b) The logarithms of σ *vs.* 1000/T of the KNM100x (M = Sb, Ta) ceramics.

and 1.79 eV, respectively. The result confirms that small amount of KNT would likely result in a significantly lower defect density, and thus promoted the fatigue resistance.

It is well demonstrated that a large unipolar strain could be obtained for compositions located at the F–R phase boundary at RT with the assistance of a relaxor-to-ferroelectric phase transition. However, as the stability of the relaxor phase depends not only on composition but also on temperature, the temperature-dependent strain was investigated in ferroelectric KNT0.5 and ergodic relaxor KNT1.25, as shown Fig. 12. For ferroelectric KNT0.5, the *P–E* loop at RT is saturated and exhibits a hysteretic shape, typical for ferroelectrics. When the temperature is increased to 80 °C above T_d (68 °C), the hysteresis loop becomes pinched, indicating the occurrence an ergodic relaxor state. The sudden change of the *P–E* loop around 80 °C coincides with the strain variation. The *S–E* curve of samples exhibits a transition from the butterfly shape to horn shape with the loss of the negative strain and a significant jump of positive strain as the temperature extends beyond T_d, confirming the FE to relaxor phase transition induced by increasing temperature. For ergodic relaxor KNT1.25, since T_d is at about RT, the room-temperature *P–E* curve already exhibits an ergodic relaxor characteristic, the *S–E* loops starts from a shape reflective of an ergodic relaxor, and only a progressive decrease of the P_r as well as *S* with increasing temperature is observed.

The variation of strain with temperature of the samples can be seen more clearly in the temperature-dependent unipolar strain hysteresis loops, as shown in Fig. 13(a) and (b). From this figure, the strain response of ferroelectric KNT0.5 shows a drastic change with temperature, and a sudden increase in the unipolar strain is observed at ~80 °C. On the other hand, ergodic relaxor ferroelectric KNT1.25 shows distinctly different behavior: continuous decreases in the strain level with the slimmer unipolar strain loops are observed as the temperature increases. Fig. 13(c) and (d) compares the variations in d^*_{33} with temperature between ferroelectric KNT0.5 and ergodic relaxor KNT1.25 materials. It is noted that the maximum d^*_{33} value for the KNT0.5 is achieved at the temperature higher than the previously indicated T_d value, because T_d is a function of electric field.[29] For the typical ferroelectric composition with KNT0.5, significant increases in d^*_{33} up to 579 pm^{-1} V are observed at temperatures higher than T_d. While for KNT1.25 samples dominated with the ergodic relaxor phase, due to the shift of T_d down to RT, a large d^*_{33} of 567 pm^{-1} V is observed at RT.

Furthermore, temperature-dependent fatigue behaviors in the present system were studied in this work. Fig. 14 shows the

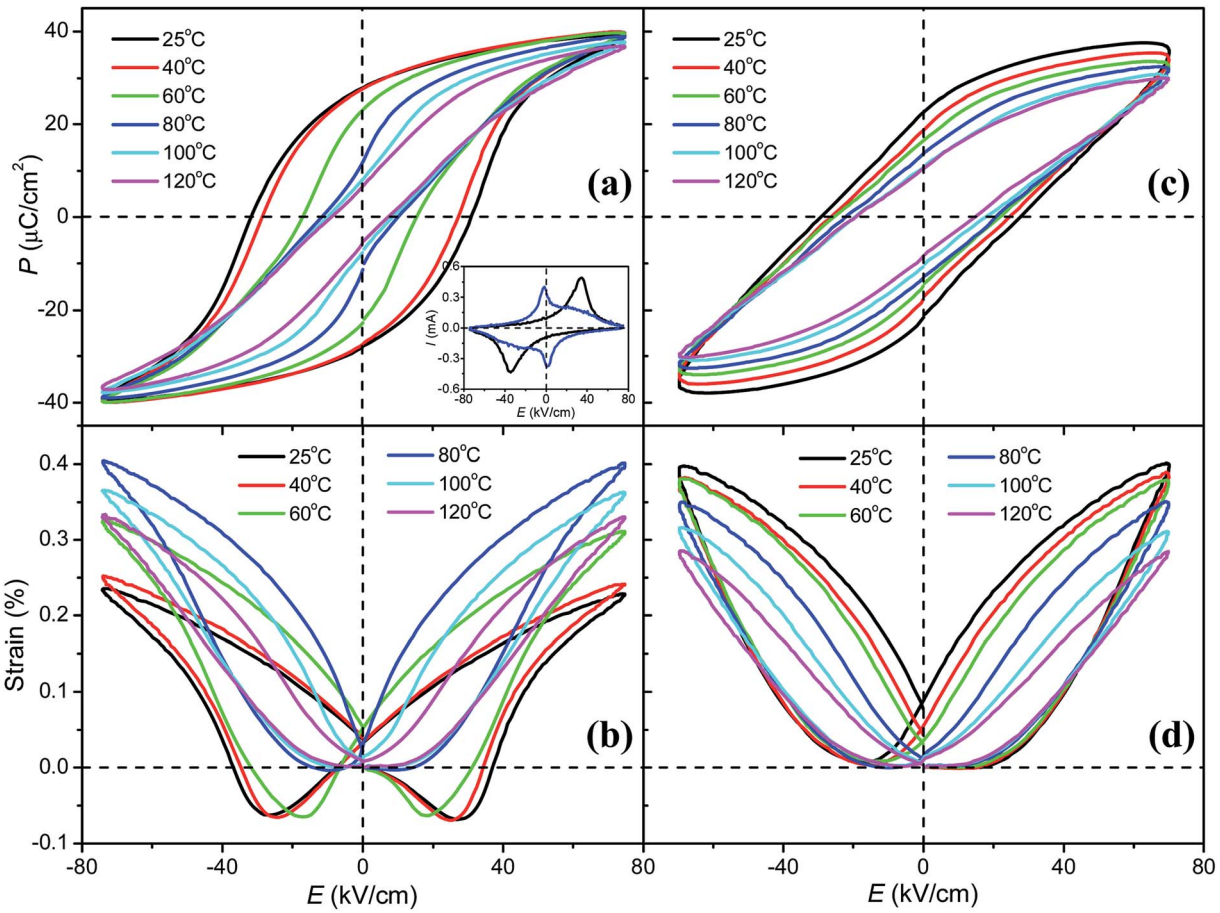

Fig. 12 Hysteresis loops and bipolar strain curves for (a), (b) ferroelectric KNT0.5 and (c), (d) ergodic relaxor KNT1.25 samples at different temperatures.

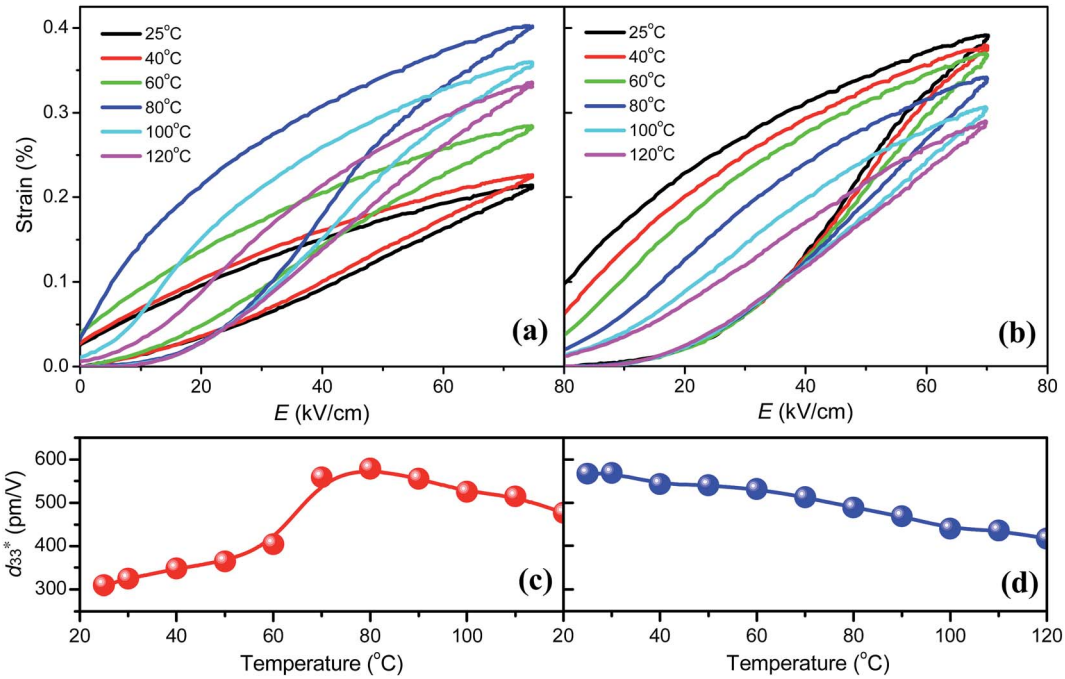

Fig. 13 Temperature-dependent unipolar strain hysteresis loops for (a) ferroelectric KNT0.5 and (b) ergodic relaxor KNT1.25 samples. Variations in d^*_{33} with temperature of (c) ferroelectric KNT0.5 and (d) ergodic relaxor KNT1.25 materials.

unipolar fatigue behavior of (a–c) ferroelectric KNT0.5 and (d–f) ergodic relaxor KNT1.25 ceramics at different temperature for 10^6 cycles. Unipolar strain at different temperature of the two samples as function of cycles is summarized in Fig. 14(g) and (h). It can be noted that both samples exhibit temperature-independent fatigue behavior: the general variation of the strain up to 10^6 cycles is within 4.5% of original value. That is the fatigue-free behavior in the present system is also insensitive to the temperature, suggesting these materials have excellent potential for demanding high cycle applications such as microelectromechanical systems actuators.

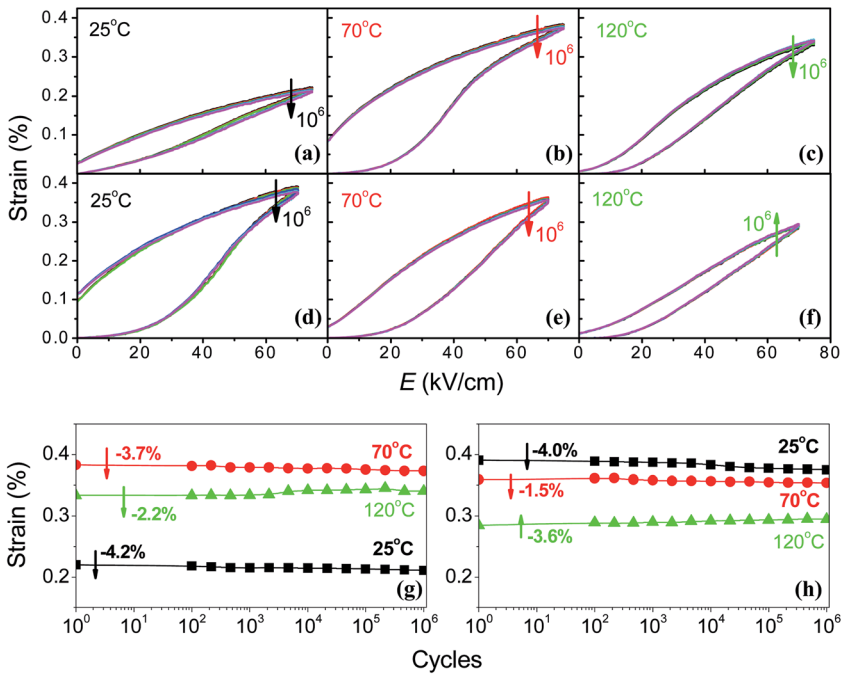

Fig. 14 Unipolar fatigue behavior of (a–c) ferroelectric KNT0.5 and (d–f) ergodic relaxor KNT1.25 ceramics at different temperature for 10^6 cycles; (g) and (h) unipolar strain at different temperature of the two samples as function of cycles.

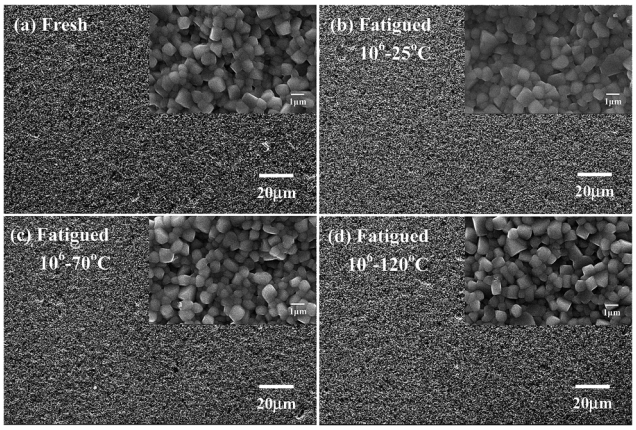

Fig. 15 SEM images from near electrode regions showing the surface of the (a) virgin sample and different temperature-fatigued specimens [(b) at 25 °C; (c) at 70 °C; (d) at 120 °C], for KNT0.5 composition. Insets are SEM micrographs of the surface of the samples at high magnification.

The appearance of cracks in the material due to long-term cyclic loading is one of the main reasons for fatigue failure of ferroelectric components. Severe crack growth is mostly induced by bipolar or electric fields with amplitudes high enough to induce polarization switching,[53] but can sometimes also be observed after unipolar electric loading.[54] In bulk ceramics, cracking often occurs close to the electrode interface and can lead to delamination of the electrodes.[55] While in the present study, samples exhibit temperature independent fatigue behavior, which indicates samples may not suffer from microstructural crack during high-temperature fatigue process. To confirm the above statement, SEM images from near electrode regions showing the surface of (a) virgin sample and (b–d) fatigued samples for KNT0.5 composition are provided, as shown in Fig. 15. No trace of microstructural crack is found during the high-temperature fatigue process. It isn't hard to understand why the present samples are restraint to filed cycling even at high temperatures. Insets are SEM micrographs of the surface of the samples at high magnification. Dense microstructures without any microstructural damage are observed even after high temperature field cycling. The grain size is uniform and only about 1.0 μm. The dense and uniform microstructure with small grain size which provides a high resistance to field cycling, may be the intrinsic reason for the fatigue-free behavior in the present system, as previously reported in the hot pressed.[56]

4. Conclusions

In summary, the effect of KNM addition on the ferroelectric behavior and piezoelectric properties of BNKT20 lead-free piezoceramics were investigated. KNM100*x* samples underwent a phase transition from ferroelectric rhombohedral and tetragonal phases to relaxor pseudocubic phase with increasing KNM content, and such transition are accompanied with the significant disruption of ferroelectric order and the shift of the ferroelectric–relaxor transition temperature T_{F-R} down to RT. Accordingly, it induced an enhancement of the field-induced strain with a peak at values of 0.39–0.41% obtained in 1.25 mol% KNM-modified samples. Temperature dependent measurements of both polarization and strain suggested that the origin of the large strain is due to a reversible field-induced ergodic relaxor to ferroelectric phase transformation. Moreover, excellent fatigue-resistant behavior was observed in the proposed KNM100*x* solid solution especially those with ergodic relaxor phase after 10^6 bipolar cycles. This finding demonstrates that these materials have excellent potential for demanding high cycle applications such as micro-electromechanical systems actuators.

Acknowledgements

This work was supported by the National Natural Science Foundation of China (No. 51402144, 51372110 and 51302124), the Project of Shandong Province Higher Educational Science and Technology Program (Grant No. J14LA11 and J14LA10), the National High Technology Research and Development Program of China (No. 2013AA030801), Science and Technology Planning Project of Guangdong Province, China (No. 2013B091000001), Independent innovation and achievement transformation in Shandong Province special, China (No. 2014CGZH0904), the Natural Science Foundation of Shandong Province of China (Grant No. ZR2014JL030), and the Research Foundation of Liaocheng University (318051407, 318011301 and 318011306).

References

1 T. R. Shrout and S. J. Zhang, *J. Electroceram.*, 2007, **19**, 113.
2 S. T. Zhang, A. B. Kounga, E. Aulbach, H. Ehrenberg and J. Rödel, *Appl. Phys. Lett.*, 2007, **91**, 112906.
3 W. Jo, T. Granzow, E. Aulbach, J. Rödel and D. Damjanovic, *J. Appl. Phys.*, 2009, **105**, 094102.
4 K. Wang, A. Hussain, W. Jo and J. Rödel, *J. Am. Ceram. Soc.*, 2012, **95**, 2241.
5 H.-S. Han, W. Jo, J.-K. Kang, C.-W. Ahn and I.-W. Kim, *J. Appl. Phys.*, 2013, **113**, 154102.
6 A. Hussain, C. W. Ahn, J. S. Lee, A. Ullah and I. W. Kim, *Sens. Actuators, A*, 2010, **158**, 84.
7 R. Z. Zuo, C. Ye, X. S. Fang and J. W. Li, *J. Eur. Ceram. Soc.*, 2008, **928**, 871.
8 W. Jo, E. Erdem, R.-A. Eichel, J. Glaum, T. Granzow, D. Damjanovic and J. Rödel, *J. Appl. Phys.*, 2010, **108**, 014110.
9 K.-N. Pham, A. Hussain, C. W. Ahn, I. W. Kim, S. J. Jeong and J. S. Lee, *Mater. Lett.*, 2010, **64**, 2219.
10 K. T. P. Seifert, W. Jo and J. Rödel, *J. Am. Ceram. Soc.*, 2010, **93**, 1392.
11 W. F. Bai, J. H. Xi, J. Zhang, B. Shen, J. W. Zhai and H. X. Yan, *J. Eur. Ceram. Soc.*, 2015, **35**, 2489.
12 J. G. Hao, B. Shen, J. W. Zhai, C. Z. Liu, X. L. Li and X. Y. Gao, *J. Appl. Phys.*, 2013, **113**, 114106.
13 C. G. Ye, J. G. Hao, B. Shen and J. W. Zhai, *J. Am. Ceram. Soc.*, 2012, **95**, 3577.

14 J. G. Hao, B. Shen, J. W. Zhai and H. Chen, *J. Appl. Phys.*, 2014, **115**, 034101.
15 F. F. Wang, M. Xu, Y. X. Tang, T. Wang, W. Z. Shi and C. M. Leung, *J. Am. Ceram. Soc.*, 2012, **95**, 1955.
16 J. G. Hao, W. F. Bai, W. Li, B. Shen and J. W. Zhai, *J. Appl. Phys.*, 2013, **114**, 044103.
17 E. A. Patterson, D. P. Cann, J. Pokorny and I. M. Reaney, *J. Appl. Phys.*, 2012, **111**, 094105.
18 R. Dittmer, W. Jo, J. Daniels, S. Schaab and J. Rödel, *J. Am. Ceram. Soc.*, 2011, **94**, 4238.
19 A. Ullah, C. W. Ahn, A. Ullah and I. W. Kim, *Appl. Phys. Lett.*, 2013, **103**, 022906.
20 J. G. Hao, B. Shen, J. W. Zhai and H. Chen, *J. Am. Ceram. Soc.*, 2014, **97**, 1776.
21 Y. P. Guo, M. Y. Gu, H. S. Luo, Y. Liu and R. L. Withers, *Phys. Rev. B: Condens. Matter Mater. Phys.*, 2011, **83**, 054118.
22 F. Ni, L. H. Luo, W. P. Li and H. B. Chen, *J. Phys. D: Appl. Phys.*, 2012, **45**, 415103.
23 O. Muller and R. Roy, *The Major Ternary Structural Families*, Springer, New York, 1974, p. 221.
24 Y. Hiruma, H. Nagata and T. Takenaka, *Appl. Phys. Lett.*, 2009, **95**, 052903.
25 A. Sasaki, T. Chiba, Y. Mamiya and E. Otsuki, *Jpn. J. Appl. Phys.*, 1999, **38**, 5564.
26 G. A. Samara, *J. Phys.: Condens. Matter*, 2003, **15**, R367.
27 Y. Hiruma, H. Nagata and T. Takenaka, *J. Appl. Phys.*, 2008, **104**, 124106.
28 W. Jo, S. Schaab, E. Sapper, L. A. Schmitt, H. J. Kleebe, A. J. Bell and J. Rödel, *J. Appl. Phys.*, 2011, **110**, 074106.
29 E. Sapper, S. Schaab, W. Jo, T. Granzow and J. Rödel, *J. Appl. Phys.*, 2012, **111**, 014105.
30 R. F. Cheng, Z. J. Xu, R. Q. Chu, J. G. Hao, J. Du and G. R. Li, *RSC Adv.*, 2015, **5**, 41646.
31 W. Jo, J. Rödel, J. S. Lee, Y. H. Balk and C. Park, *Funct. Mater. Lett.*, 2010, **3**, 41.
32 F. Z. Yao, J. Glaum, K. Wang, W. Jo, J. Rödel and J. F. Li, *Appl. Phys. Lett.*, 2013, **103**, 192907.
33 W. Jo, R. Dittmer, M. Acosta, J. Zang, C. Groh, E. Sapper, K. Wang and J. Rödel, *J. Electroceram.*, 2012, **29**, 71.
34 Z. H. Luo, T. Granzow, J. L. Glaum, W. Jo, J. Rödel and M. Hoffman, *J. Am. Ceram. Soc.*, 2011, **94**, 3927.
35 M. Ehmke, J. Glaum, W. Jo, T. Granzow and J. Rödel, *J. Am. Ceram. Soc.*, 2011, **94**, 2473.
36 E. A. Patterson and D. P. Cann, *Appl. Phys. Lett.*, 2012, **101**, 042905.
37 C. Y. Tian, F. F. Wang, X. Ye, Y. Q. Xie, T. Wang, Y. X. Tang, D. Z. Sun and W. Z. Shi, *Scr. Mater.*, 2014, **83**, 25.
38 Y. Li, F. F. Wang, X. Ye, Y. Q. Xie, Y. X. Tang, D. Z. Sun, W. Z. Shi, X. Y. Zhao and H. S. Luo, *J. Am. Ceram. Soc.*, 2014, **97**, 3615.
39 W. Pan, C. F. Yue and O. Tosyali, *J. Am. Ceram. Soc.*, 1992, **75**, 1534.
40 N. Balke, H. Kungl, T. Granzow, D. C. Lupascu, M. J. Hoffmann and J. Rödel, *J. Am. Ceram. Soc.*, 2007, **90**, 3869.
41 N. Balke, D. C. Lupascu, T. Granzow and J. Rödel, *J. Am. Ceram. Soc.*, 2007, **90**, 1081.
42 N. Balke, D. C. Lupascu, T. Granzow and J. Rödel, *J. Am. Ceram. Soc.*, 2007, **90**, 1088.
43 J. Nuffer, D. C. Lupascu, A. Glazounov, H. J. Kleebe and J. Rödel, *J. Eur. Ceram. Soc.*, 2002, **22**, 2133.
44 Z. Luo, J. Glaum, T. Granzow, W. Jo, R. Dittmer, M. Hoffman and J. Rödel, *J. Am. Ceram. Soc.*, 2011, **94**, 529.
45 M. Ehmke, J. Glaum, W. Jo, T. Granzow and J. Rödel, *J. Am. Ceram. Soc.*, 2011, **94**, 2473.
46 N. Kumar and D. P. Cann, *J. Appl. Phys.*, 2013, **114**, 054102.
47 Z. Luo, T. Granzow, J. Glaum, W. Jo, J. Rödel and M. Hoffman, *J. Am. Ceram. Soc.*, 2011, **94**, 3927.
48 J. G. Hao, Z. J. Xu, R. Q. Chu, W. Li and J. Du, *J. Alloys Compd.*, 2015, **647**, 857.
49 D. C. Sinclair and A. R. West, *J. Appl. Phys.*, 1989, **66**, 3850.
50 M. Boukriba, F. Sediri and N. Gharbi, *Mater. Res. Bull.*, 2013, **48**, 574.
51 B. S. Kang, S. K. Chol and C. H. Park, *J. Appl. Phys.*, 2003, **49**, 1904.
52 J. J. Dih and R. M. Fulrath, *J. Am. Ceram. Soc.*, 1978, **61**, 448.
53 H. Weitzinger, G. A. Schneider, J. Steffens, M. Hammer and M. J. Hoffmann, *J. Eur. Ceram. Soc.*, 1999, **19**, 1333.
54 J. Glaum, T. Granzow, L. A. Schmitt, H.-J. Kleebe and J. Rödel, *Acta Mater.*, 2011, **59**, 6083.
55 Q. Y. Jiang and L. E. Cross, *J. Mater. Sci.*, 1993, **28**, 4536.
56 Q. Y. Jiang, E. C. Subbarao and L. E. Cross, *Acta. Metall. Mater.*, 1994, **42**, 3687.

